Cellulose triacetate/LUDOX-SiO_2 nanocomposite for pervaporation desalination membrane

Indah Prihatiningtyas*[1,2], Yusak Hartanto[3], Maria Sandra Reyes Ballesteros[1], and Bart Van der Bruggen*[1,4]

[1]*Department of Chemical Engineering, KU Leuven, Celestijnenlaan 200F, B-3001, Leuven, Belgium*

[2]*Department of Chemical Engineering, Mulawarman University, Jalan Sambaliung No.9, Sempaja Selatan, Samarinda, Kalimantan Timur, Indonesia*

[3]*Materials and Process Engineering (iMMC-IMAP), UC Louvain, Place Sainte Barbe 2, 1348 Louvain-la-Neuve, Belgium.*

[4]*Faculty of Engineering and the Built Environment, Tshwane University of Technology, Private Bag X680, Pretoria 0001, South Africa*

*Corresponding authors: bart.vanderbruggen@kuleuven.be; indahprihatiningtyas.yamsidi@kuleuven.be

Abstract

A series of cellulose triacetate/Ludox-silica nancomposite pervaporation membranes was successfully prepared via solution casting, aiming to improve the performance of cellulose triacetate membranes for desalination. The fabricated nanocomposite membranes were characterized to study the membrane morphology, chemical composition, mechanical properties, and surface hydrophilicity. Furthermore, the desalination performance was investigated as a function of silica (SiO_2) loading (ranging from 1 to 4 wt.%) and feed concentration at 30 g/L and 60 g/L of sodium chloride (NaCl). Pervaporation experiments showed that incorporating 4 wt.% SiO_2 into a cellulose triacetate (CTA) membrane increased the water flux by a factor 2.5 compared to pristine CTA (from 2.2 kg m^{-2} h^{-1} to 6.1 kg m^{-2} h^{-1}) for a 30 g/L NaCl feed solution at 70°C, while the salt rejection remained above 99 %. The CTA/4 wt.% SiO_2 membrane was found to have only 21 % flux reduction when tested with a 60 g/L NaCl feed solution, without changes in membrane selectivity. This suggests that the developed CTA/Ludox-SiO_2 nanocomposite pervaporation membrane is suitable for desalination.

Keywords: Nanocomposite; pervaporation; cellulose triacetate; ludox-SiO_2; desalination

INTRODUCTION

Anthropogenic activities and human population growth have caused water pollution, groundwater exploitation, and increasing water consumption, which leads to fresh water scarcity [1]. Seawater desalination has become a growing practice in many parts of the world to resolve this issue as almost 97% of the world water resources are seawater. Reverse osmosis (RO) is currently the most established membrane desalination technology worldwide with the majority of the installed capacity, due to its high energy efficiency in comparison with conventional thermal desalination processes [2]. However, the high applied pressure in RO, especially at elevated feed salinity, results in an unfavorable high operating cost. RO also needs extensive feed pre-treatment due to the high susceptibility of the RO membranes to fouling and inorganic scaling, so that this technology is still relatively expensive to produce fresh water [3].

Alternative membrane-based desalination processes aiming to integrate waste heat utilization or solar energy to drive the separation process, such as forward osmosis (FO) [4] and membrane distillation (MD) [5], have been developed to address the aforementioned RO desalination issues. However, FO is facing significant challenges in finding effective and easily regenerable draw solution materials [6–8] while MD often has a high fouling propensity due to the use of hydrophobic membranes [9]. In recent years, there has been a growing interest in applying pervaporation (PV) as a desalination process due to its high salt rejection performance [10,11], often without the need for extensive feed solution pre-treatment since hydrophilic membranes are used, leading to a lower membrane fouling propensity. In addition, PV is able to treat feed waters with high salinity without significantly losing the membrane selectivity. Therefore, PV would be a cost competitive desalination technology if tailored PV membranes having a high water permeability without compromising the salt selectivity would be available in the market.

Polymer-based membranes are currently used as state-of-the-art PV technology due to their simple fabrication process, low manufacturing costs and excellent mechanical properties. For example, cellulose ester-based polymer, such as cellulose triacetate, have been widely applied as membrane materials due to its excellent salt rejection properties [12]. Nevertheless, pristine cellulose triacetate PV membranes usually suffer from a low water flux due to the dense membrane morphology [10] . One way to improve the membrane performance in PV is to develop nanocomposite membranes by incorporating inorganic or organic nanoparticles (NPs) into the polymer matrix. Several inorganic and organic nanofillers, such as TiO_2 [13–16], SiO_2 [17–19], Al_2O_3 [20,21], graphene oxide [22,23], carbon nanotubes [24,25], nanoclays [26] and cellulose nanocrystals [27,28] have been used to prepare nanocomposite membranes. Although cellulose-based nanocomposite membranes have been developed for PV process, these membranes have only been evaluated for organic-organic mixtures [29–31] and solvent dehydration applications [32,33]. To date, there is no study has investigated the CTA/silica nanocomposite membranes for pervaporation desalination process [34,35].

In this study, nanocomposite PV membranes prepared via solution casting from commercially available materials, i.e., cellulose triacetate (CTA) and colloidal Ludox-SiO_2 nanoparticles. CTA was chosen as polymer matrix due to its high salt rejection, excellent mechanical and chemical properties strength, low cost, low fouling tendency and the fact that it can be processed to yield dense films. On the other hand, silica nanoparticles were selected as nanofillers due to their attractive properties such as low toxicity, hydrophilic and excellent mechanical enhancement properties. A series of nanocomposite CTA/Ludox-SiO_2 membranes was prepared and characterized in terms of water flux and salt rejection.

EXPERIMENTAL

Materials

Cellulose triacetate (CTA, acetyl content 43 – 44%, molecular weight 966.846 g/mol, Across Organics TM, China), and dimethyl sulfoxide (DMSO, 99% pure) were purchased from Honeywell, Japan. Colloidal silica, LUDOX AS-40 (40 wt.% SiO_2 suspension in water), with surface area 135 m^2/g was obtained from Sigma Aldrich. Sodium chloride (NaCl, 99.5% purity) from Across Organics was dissolved in MilliQ water used as a feed solution for the pervaporation experiments.

Preparation CTA/Ludox-SiO_2 nanocomposite membranes

CTA/Ludox-SiO_2 nanocomposite membranes were fabricated by first dispersing LUDOX AS-40 in DMSO. LUDOX AS-40 colloidal is a commercial suspension containing silica 40 wt.% in water. A series of LUDOX AS-40 suspensions was prepared based on a different weight percentage of SiO_2 (1 wt.%, 2 wt.%, 3 wt.% and 4 wt.%) in dope solutions. The calculation based on the solid content of SiO_2 in the dope solution (supporting information). The LUDOX dispersion was then stirred at a speed of 1,000 rpm for 3 h at 70^{o}C. Subsequently, 6 wt.% of CTA solid polymer was added to the LUDOX dispersion and stirred for another 3 h at 70^{o}C. The dope solution was then sonicated for 2 h and was stirred overnight. The dope solution was left for another 2 h in the fume hood to remove air bubbles formed during the stirring. The dope solution was casted onto glass plates at room temperature and at the relative humidity of 35%. The casting knife height was set at 200 µm and the casting speed was 0.09 cm/s. It was then immediately placed in a vacuum oven set at 60^{o}C for 4 h to evaporate the solvent. The dried membranes were peeled from the glass plate by immersing it into a water bath. The maximum SiO_2 loading was 4 wt.% because adding 5 wt.% SiO_2 in the dope solution leads to a dope solution with a very low viscosity. As a consequence, the membrane film stuck

to the glass plate after solvent evaporation, so that the membrane was easily broken when it was peeled from the glass plate.

Pore size distribution

Pore size distribution of SiO_2 nanoparticles was measured using surface area and pore size analyzer (Nova 2000e, Quantachrome and Anton Paar, USA). A Brunauer–Emmett–Teller (BET) technique was used to measure the surface area and pore size distribution. The SiO_2 nanoparticle samples were prepared by evaporating the suspension of SiO_2 (Ludox As-40) to recover solid SiO_2 nanoparticles.

Particle size analysis

A particle analyzer (Nanoplus 3-Zeta/nano particle analyzer, USA) was used to characterize the particle size and particle size distribution of SiO_2 nanoparticles in the dispersions. The Nanoplus is capable to measure the particle size in the range of 0.1 nm to 12.30 µm in a concentration range of up to 40% w/v, and a sensitivity for molecular weight as low as 250 Da.

Electron Microscopy

Scanning electron microscopy (SEM) (Philips XL30 SEM, the Netherlands) analysis was performed to observe the surface and cross-sectional membrane morphology of the membranes. Each sample was sputter-coated with a thin layer of gold under vacuum to prompt conductivity before examining. The samples were fractured in cryogenic liquid nitrogen before obtaining cross section images.

Fourier Transform Infrared Spectroscopy

Fourier transform infrared spectroscopy (ATR-FTIR, Perkin Elmer, spectrum 100, USA) was used to characterize the chemical composition of the pristine CTA and the change of the

chemistry of CTA/ Ludox-SiO_2 nanocomposite membrane in the range of 4000-650 cm^{-1}. Resolution used was 4 with 4 scanning. The procedure is following : the ATR platform is first cleaned to remove any residuals and the background measurement is taken. Then the sample membrane is placed on the platform and the compression head is pressed against the membrane up to a safe value of pressing force. Once the live transmission plot has stabilized the measurement scans are carried out. After this the sample is removed and the platform and the compression head were cleaned.

Contact angle measurements

Contact angle measurements were conducted to determine the surface hydrophilicity of the membranes. A low contact angle indicates a high water affinity, which refers to a hydrophilic membrane. [36] Contact angle measurements were measured using a standard contact angle apparatus (Krüss GmbH Germany, model: DSA 10-Mk2), employing a drop-shape analysis software to study the video images of the water pendant drops. A syringe plunger was used for dropping 2 µL of water at rate of 24.79 µL/min on the surface of the membrane at room temperature.

Mechanical properties

A tensile test using a mini tensile/compression machine, model: Instron 5943 was used to measure the mechanical strength of the CTA/Ludox-SiO2 membrane. At least 4 specimens with width of 10 mm and length of 10 mm were snipped into a rectangular shape in ambient condition.

Performance of CTA/Ludox-SiO_2 PV nanocomposite membranes for desalination

The performance of CTA/Ludox-SiO_2 nanocomposite membranes was investigated in a laboratory scale setup as shown schematically in **Figure 1**. The CTA/Ludox-SiO_2 membrane was placed in a stainless-steel module with an effective membrane area of 19.625 cm^2. The

feed was heated at 70 °C and was circulated with a pump into the membrane module at a flowrate of ± 60-80 L/h. A vacuum pump with low pressure below 1 mbar was applied at the permeate side create the vapor pressure difference across the membrane. The permeate vapor was collected in a cold trap using a double U-shaped glass tube immersed in liquid nitrogen. The experiments were running continuously for 2 h. The membrane performance is determined by the water flux and rejection as follows. [8]

$$J_w = \frac{m}{(A.t)} \quad (1)$$

$$R(\%) = \left(1 - \frac{C_p}{C_f}\right) x\ 100\% \quad (2)$$

where J_w is the water flux, m is the mass of permeate obtained (kg), A is the membrane area (m^2) and t is the working time (h). The salinity of water was measured by a Consort model C831-conductivity meter. The salt rejections ($R, \%$), where C_p and C_f are the salinity in the permeate and feed solutions, respectively.

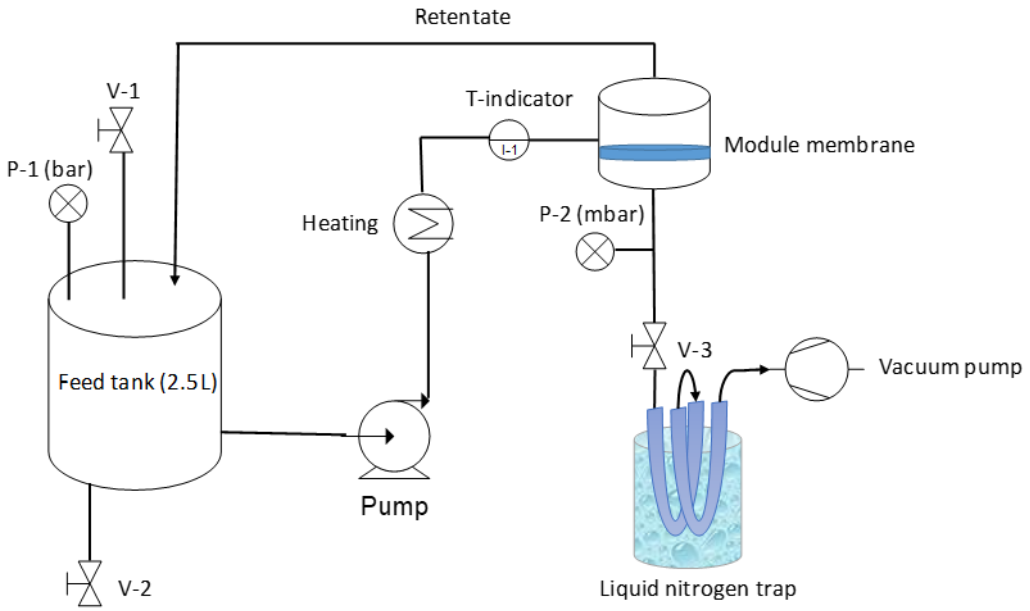

Figure 1. Schematic laboratory scale apparatus for pervaporation membrane desalination process.

RESULT AND DISCUSSION

Pore size distribution

The specific surface area of solid SiO_2 nanoparticles was calculated using the multipoint BET-equation. Figure 2a shows the BET plot of SiO_2 nanoparticles and the specific surface area is 126.620 m^2/g. While the pore size distribution of SiO_2 was measured by BJH method. The results of BJH adsorption is shown in Figure 2b. The curve of Figure 2b reveals that the pore size diameter of SiO_2 is in the range of 1.4 nm (14.86A°) to 6.9 nm (69.62A°). The average pore size diameter calculated from BJH method is 2.9 nm (29.71A°), which indicating the pore size is in the mesoporous range (2 – 50 nm). [37]

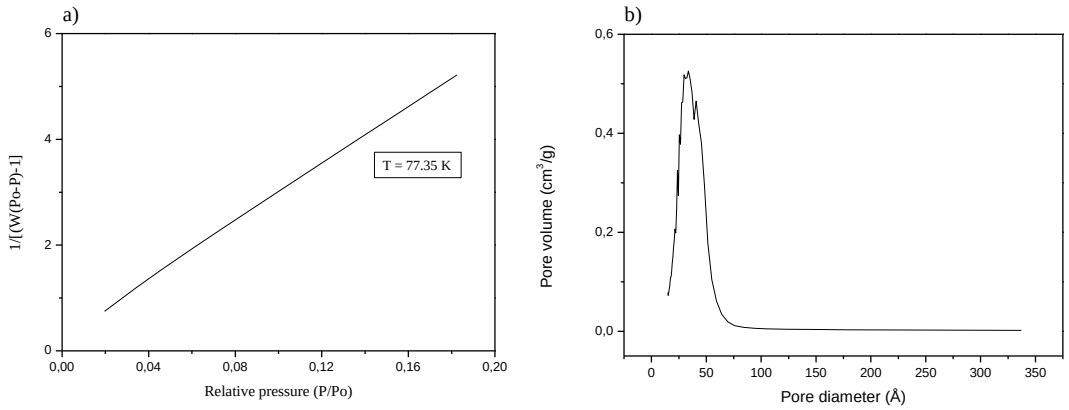

Figure 2. (a) BET result. (b) BJH pore size distribution curves of SiO_2 nanoparticles.

Particle size analysis in solution.

Figure 3 shows the particle size distribution of the original colloidal SiO_2 (LUDOX AS-40) dispersion and the particle size distributions of SiO_2 when it was mixed with DMSO for different concentrations. As shown in Figure 3a, the mean particle size of the initial SiO_2 (LUDOX AS-40) is 41 nm. However, there was some agglomeration of SiO_2 when it was dispersed in DMSO. As shown in Figure 3b-e, the particle size of SiO_2 increases as the particle concentration in DMSO increases. The results of the particle size analyzer show that the mean particle size with 1 wt.% SiO_2 in the DMSO solution was 3.35 µm and 0.97 µm, 12.9 µm, 3.17

µm, respectively, for 2 wt.%, 3 wt.%, and 4 wt.% (see Figure 2b-e). The agglomeration of SiO_2 nanoparticles is due to the interactions between individual nanoparticles, dominated by two major forces, i.e., the intermolecular force (Van der Waals force) and the electrostatic force. [38] Often, the intermolecular force has more pronounced effect than the electrostatic force (repulsive force). [39] The larger main particle size of 3 wt.% SiO_2 in DMSO compared to those of 1 wt.%, 2 wt.% and 4 wt.% might be attributed to the effect of dispersion on the aggregation nanoparticles. An aqueous solution containing SiO_2 nanoparticles (40% SiO_2 in water) was added into DMSO, and loaded SiO_2 will lead to a less viscous dispersion compared to CTA dope solution (See Figure S2). Figure S2 shows that increasing SiO_2 is not significantly increasing the viscosity, while dope solution 3 wt.% of SiO_2 is not showing the result due to there was agglomeration in the dope solution.

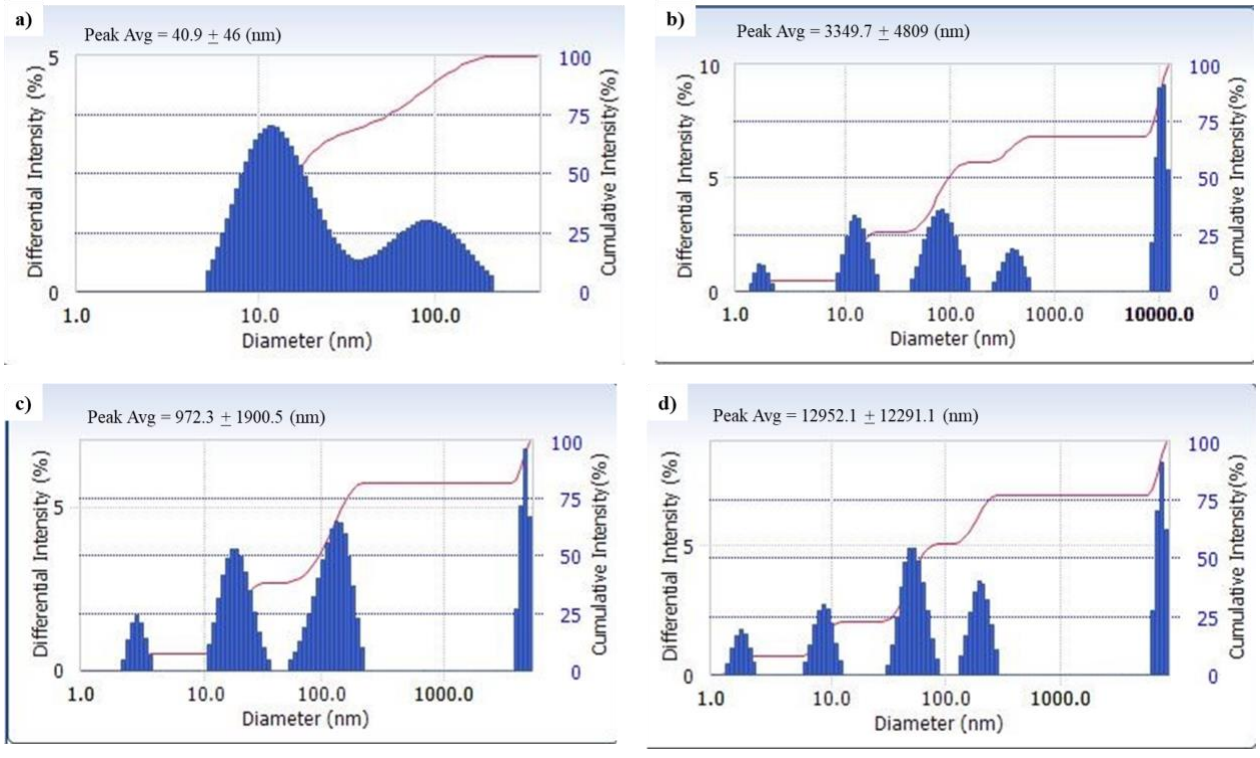

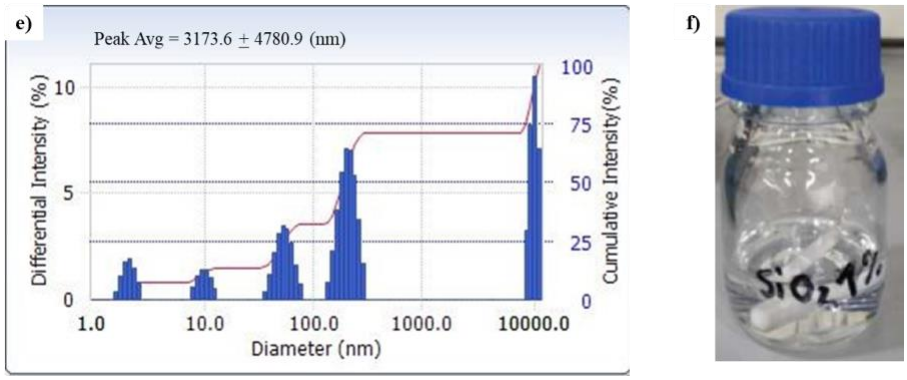

Figure 3. Particle size distributions, (a) initial SiO_2 (LUDOX AS-40); SiO_2 in DMSO at different concentrations (b) 1 wt.% SiO_2 , (c) 2 wt.% SiO_2, (d) 3 wt.% SiO_2, (e) 4 wt.% SiO_2, and (f) photograph of the solution SiO_2 in DMSO.

Ludox is a colloidal SiO_2 dispersion in which SiO_2 particles form a stable dispersion, as shown in Figure 3a. Nevertheless, the agglomeration of SiO_2 started when 1 wt.% of SiO_2 in colloidal form was added to DMSO. Figure 3c shows that the aggregation of the colloidal solution containing 2 wt.%-SiO_2 in DMSO resulted in the smallest mean particle size and the particle size distribution was more uniform compared to 1 wt.%, 3 wt.% and 4 wt.% (see Figure 3b, 3d, and 3e). This indicates that 2 wt.%-SiO_2 in DMSO has a higher intraparticle repulsive force, leading to less agglomeration. Nonetheless, all ludox-SiO_2 in DMSO dispersion has a transparent appearance (see Figure 3f).

Morphological characterization

SEM images shown in Figure 4a-e suggest a dense membrane surface for all the fabricated membranes. The incorporation of SiO_2 in the CTA membrane can be seen as a white spot on the membrane surface (see Figure 4b-e). As shown in Figure 4c, adding 2 wt.% of SiO_2 nanoparticles results in numerous protrusions on the membrane surface, possibly due to the aggregation of SiO_2. It can be seen in Figure 3c that the smallest mean particle size is obtained when 2 wt.% SiO_2 was dispersed into DMSO; smaller particles have a higher interfacial area

and potentially tend to aggregate, which led to the highest roughness among all prepared membranes [41]. Although there was some aggregation of nanoparticles on the membrane surface, the aggregation appeared homogeneous and uniform due the intrinsic characteristics of the colloidal SiO_2 which was dispersed well in the solution (Figure 3f). The cross-section image of the pristine membrane (Figure 4f) shows that it adopts a sponge-like structure with dense top and bottom layers. As the concentration of SiO_2 increased, the cross-section membrane morphology changes from porous middle layer to uniform dense structure (Figure 4g-j). It seems that the SiO_2 nanoparticles filled the pores in the sponge-like structure for CTA/SiO_2 nanoparticles membranes, resulting in a dense structure. Furthermore, increasing the SiO_2 loading leads to an increase in the final membrane thickness, as shown in Table 1.

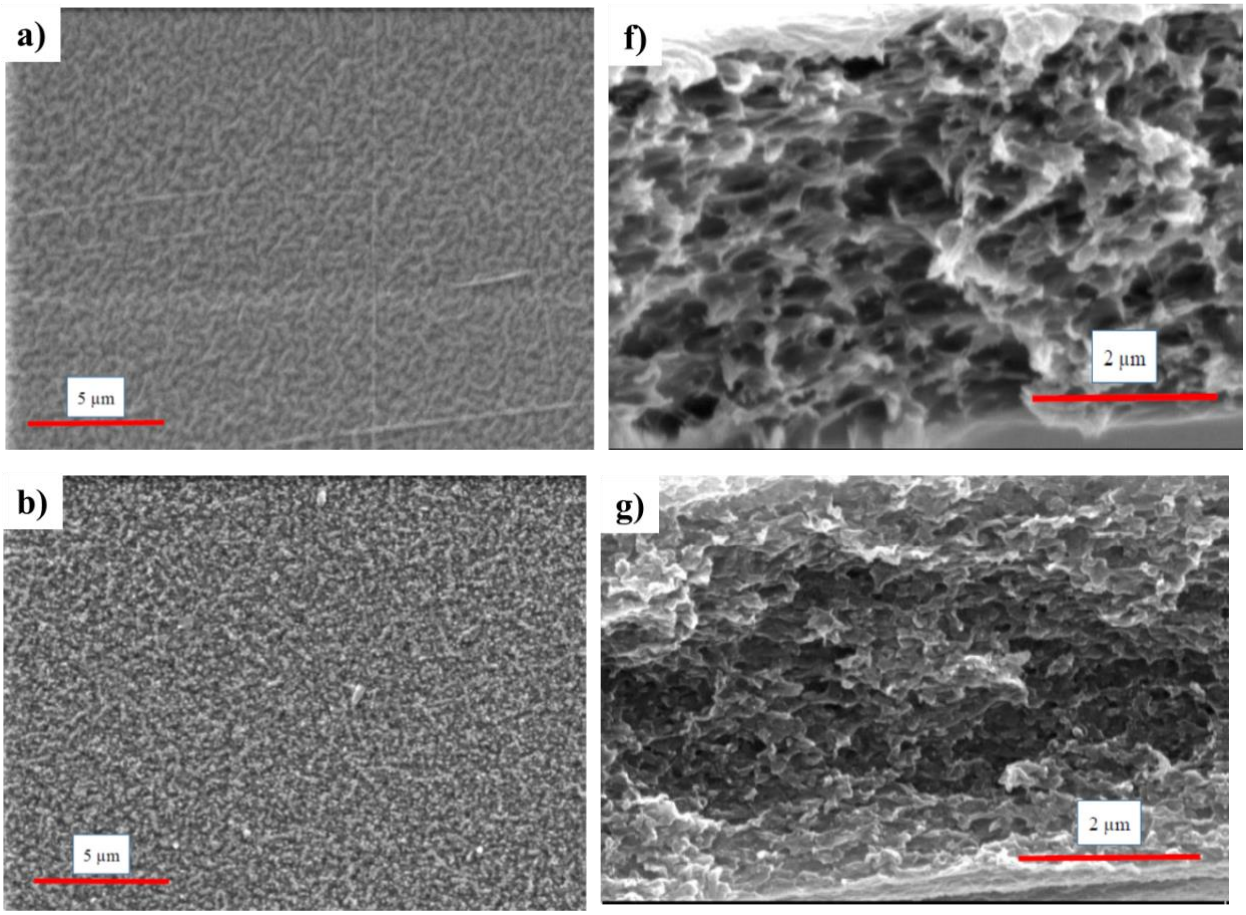

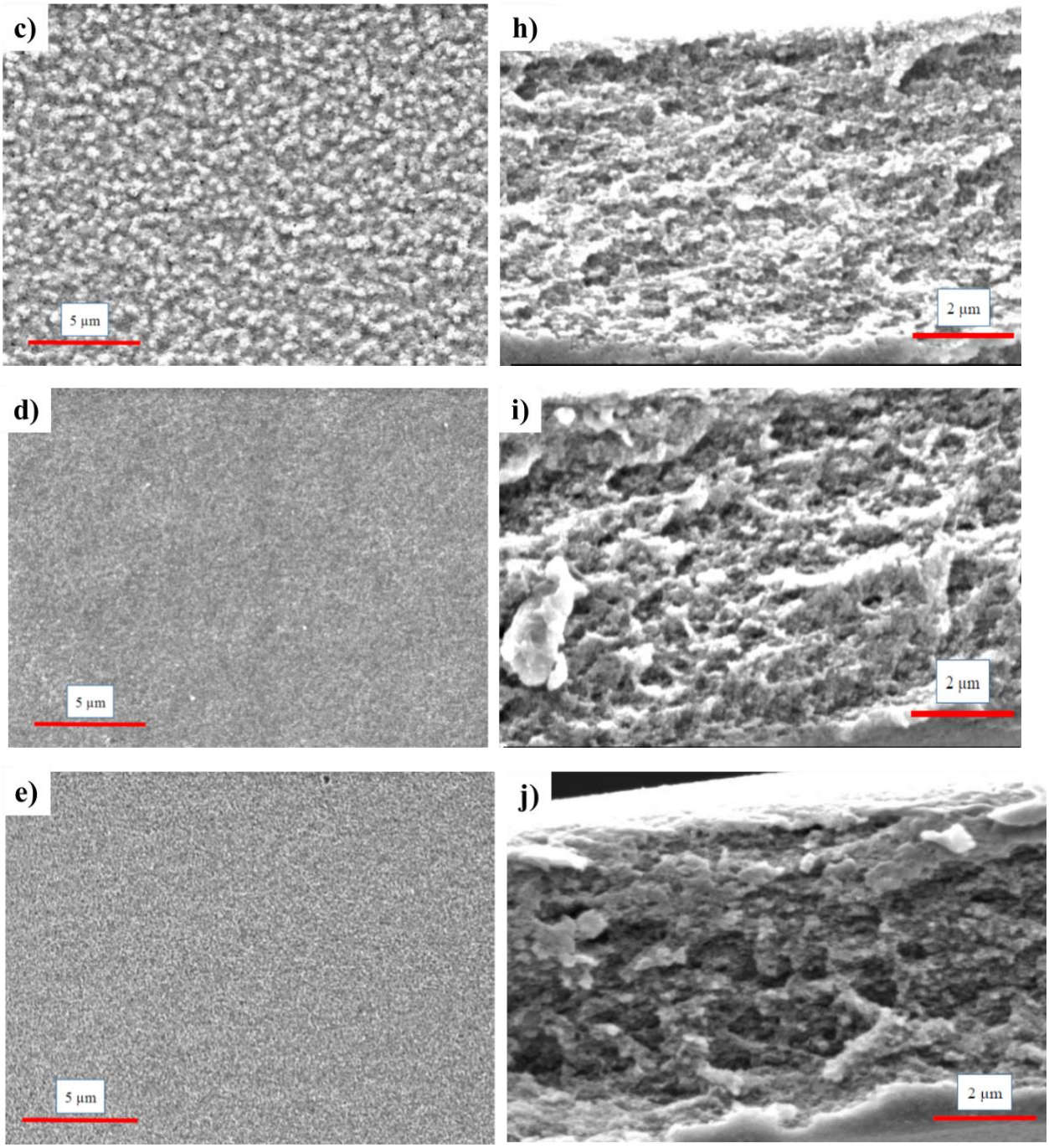

Figure 4. SEM images of membrane surface (a) CTA pristine, (b) CTA-1wt.% SiO_2, (c) CTA-2wt.% SiO_2, (d) CTA-3wt.% SiO_2, (e) CTA-4wt.% SiO_2 (magnification 5000x), the cross-section (f) CTA pristine, (g) CTA-1wt.% SiO_2, (h) CTA-2wt.% SiO_2, (i) CTA-3wt.% SiO_2, (j) CTA-4wt.% SiO_2 (magnification 10,000x) of nanocomposite membrane, and (k) the thickness of the prepared membranes.

Table 1. Thickness of the membranes

% weight of SiO_2	Modus (mm)	Average (mm)	Error
0	0.006	0.0066	0.00089
1	0.009	0.0088	0.00098
2	0.008	0.0084	0.00089
3	0.009	0.0092	0.0005
4	0.01	0.01	0.00081

FTIR Characterization

The surface functional group characterization of CTA/SiO_2 nanocomposite membranes by FTIR is shown in Figure 5. Most of the characteristic peaks in this figure are related to the pristine CTA membrane. The peak at 1370 cm^{-1} is attributed to the asymmetric bending of C-H, the peak 1216 cm^{-1} belongs to C-O stretching and the peak at 1023 cm^{-1} corresponds to pyranose ring C-O-C stretching (see Figure 5a). As Figure 5b shows, the characteristic peaks at 2963 cm^{-1} and 3484 cm^{-1} are corresponding to the stretching vibration of C-H and O-H, respectively. [42] Compared with the pristine CTA membrane, the new peaks at 798 cm^{-1} and 1121 cm^{-1} (see Figure 5a) represents the Si-O bending and Si-O- Si symmetric stretching. [43,44] The decreasing percentage of peak transmittance at 798 cm^{-1} and 1121 cm^{-1} correlates to the higher SiO_2 content in the membrane. The FTIR results confirm that SiO_2 nanoparticles are present in the fabricated nanocomposite membranes.

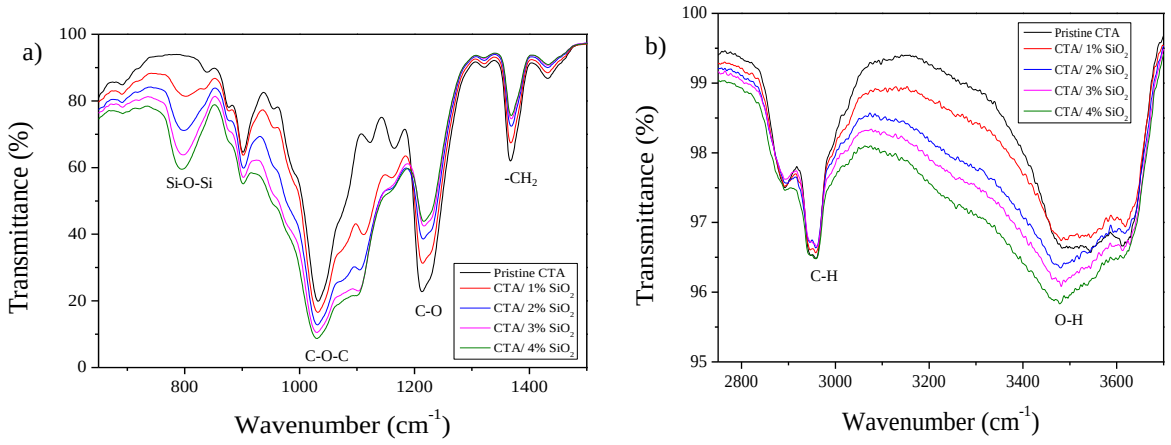

Figure 5. FTIR spectra of CTA/SiO_2 nanocomposite membranes fabricated in different content of SiO_2, (a) Wavenumber range in 650 to 1500 cm^{-1}, and (b) Wavenumber range in 2750 to 3700 cm^{-1}.

Contact angle and mechanical properties analysis

Figure 6a presents the water contact angle values of the nanocomposite membranes with different SiO_2 content. All fabricated membranes are hydrophilic with a contact angle between 56.8-68.9° as shown in Fig.6a. Increment of SiO_2 content does not have any significant impact on the surface hydrophilicity. However, loading 2 wt.% SiO_2 in CTA membrane resulted in a hydrophilicity improvement due to roughness on the membrane surface (see Figure 4c). Generally, there are two wetting models which suggested to explain the relationship between surface roughness and the contact angle of the surface, i.e the Wenzel [45] and Cassie-Baxter [46] models. Wenzel equation states that the surface roughness enhances both hydrophilicity and hydrophobicity, which is dependent on the nature of the material surface. CTA/SiO_2 is a hydrophilic membrane, hence with the increase in surface roughness will enhance the hydrophilicity of the membrane

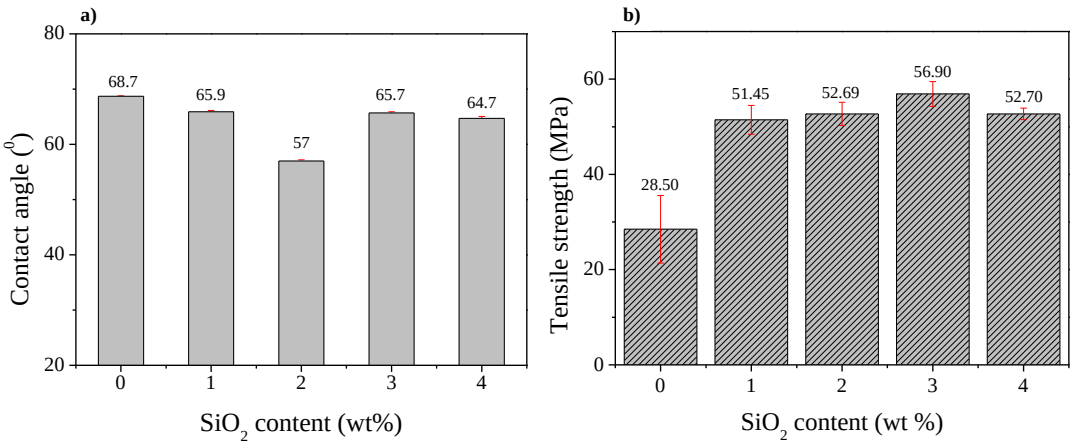

Figure 6. Contact angle of CTA/SiO_2 nanocomposite membranes (a), and tensile strength (b) with different SiO_2 content.

Figure 6b shows that the SiO_2 incorporation significantly enhances the membrane tensile strength. Salahshoori et.al noted that incorporating of SiO_2 nanoparticle in the membrane will enhance the tensile strength of the pristine membrane due to the uniform distribution of SiO_2 nanoparticles in the membranes [47]. This is in agreement with the morphological characterization in Figure 4, indicating that the uniform silica nanoparticle distribution increases nanocomposite membrane tensile strength. Besides, SiO_2 nanoparticles play a role as physical transfusion coupling between polymer parts, which reduces cracks or cavities at the membrane weak points [48]. However, increasing SiO_2 content beyond 3 wt.% has an adverse effect on membrane tensile strength. Salahshoori reported that at percentages of SiO_2 was more than 15 wt.% in Polysulfone (PSF) membrane, the tensile strength decreased due to the accumulation of SiO_2 particles in PSF membrane.[47]

These results imply that the presence of SiO_2 as inorganic nanoparticles strengthens the nanocomposite membrane due to the good dispersion of SiO_2 nanoparticles and the solid interaction between SiO_2 nanoparticles with the CTA matrix [49]. Therefore, the interfacial interaction between inorganic nanoparticles and polymer matrix should be considered an important factor affecting the tensile strength; however, excessive amounts of particles loaded would initiate the tensile strength to be decreased [50].

Pervaporation desalination performance

Figure 7 shows the effect of SiO_2 content on the membrane permeability and NaCl rejection. The PV performance of CTA/SiO_2 membranes in different SiO_2 content were investigated using a feed solution with a concentration of 30 g/L NaCl at a temperature of 70°C. Figure 7a shows that increasing the concentration of SiO_2 nanoparticles in the CTA membrane increases the water flux without sacrificing the NaCl rejection, as the NaCl removal stays above 99%. The highest water flux was obtained with a CTA/4wt.% SiO_2 nanocomposite membrane at 6.1

kg m^{-2} h^{-1}. The water flux of the CTA/4% SiO_2 nanocomposite membrane can be increased by a factor 2.5 compared to the pristine CTA membrane. This increment is due to the addition of SiO_2 into the CTA membranes, which increases the hydrophilicity as described in FTIR spectra (see Figure 5.b), as indicated by the hydroxyl group improvement. The membrane hydrophilic surface will enhance the water flux due to more water molecules being absorbed into the membrane. [51,52] As shown in Figure 1b that diameter SiO_2 nanoparticles has diameter pore size is 2.9 nm. Hence, incorporating SiO_2 nanoparticles into CTA membrane can provide additional permeation pathways, which also contribute to the higher water flux. Figure 8 presents a schematic of SiO_2 in the dense polymer matrix. Salt rejection can be maintained above 99% because of the role of the dense structure on the membrane surface of CTA/SiO_2 which acts as a selective layer. Besides, the high salt rejection due to non-volatility and low diffusivity of NaCl. [53–55]

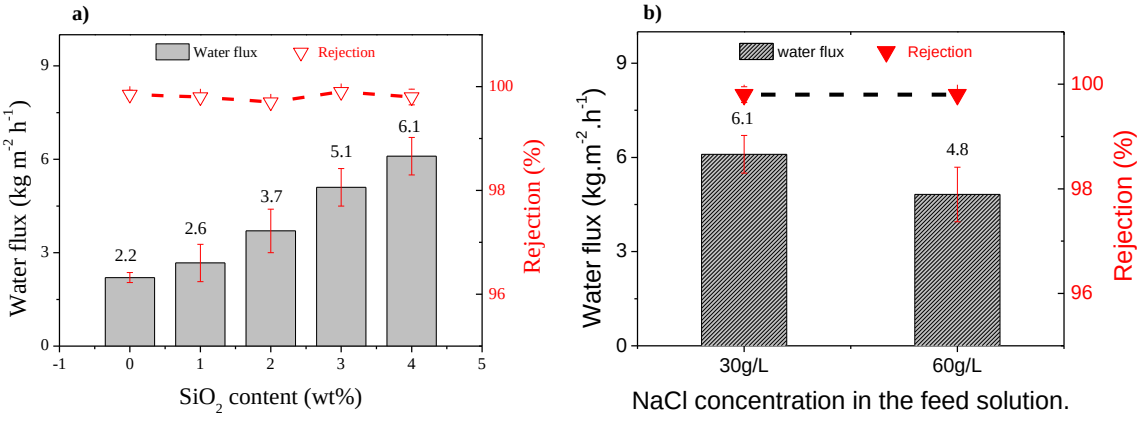

Figure 7. Pervaporation performance of CTA/SiO_2 nanocomposite membranes fabricated in different content SiO_2 (a), and pervaporation performance of CTA/4% SiO_2 nanocomposite membrane at different NaCl concentrations (b).

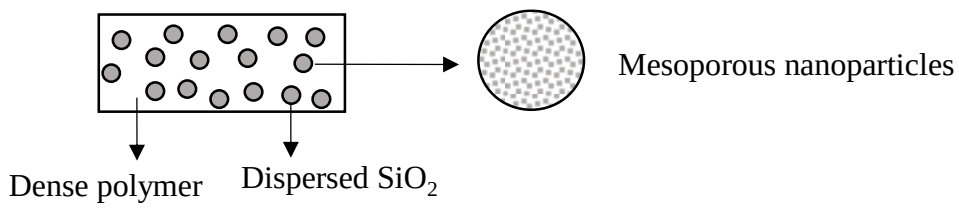

Figure 8. A schematic of SiO_2 in the dense polymer matrix

Figure 7b shows the effect of the NaCl concentration in the feed on the performance of the CTA/4wt.% SiO_2 nanocomposite membrane at 70°C. The water flux decreased by 21% (6.1 kg m^{-2} h^{-1} to 4.8 kg m^{-2} h^{-1}) when the NaCl concentration of the feed solution increased from 30 g/L to 60 g/L NaCl; however, the NaCl rejection was independent of the feed concentration.

Increasing feed concentration tends to increase the concentration of species in the membrane. Feed concentration influences the sorption of species at the membrane interface. [56] Fick's law equation explains that flux (J) and diffusion (D) are concentration dependent (dc).[10]

$$J = D \frac{d_c}{d_x} \quad (3)$$

While Antoine equation states that the vapor pressure (P) of water increased with temperature (T).[57]

$$Log\ P = A - \frac{B}{T} \quad (4)$$

However, the decrease of water concentration at room temperature will not have significant effect on the water diffusivity in the membrane matrix. Hence, the difference in water vapor pressure at room temperature is negligible, while at temperature above 65 ^{0}C the increasing temperature is more significant.[53] At high temperature (70 ^{0}C) the vapor pressure enhances along with increasing the temperature. Differences in bulk feed water concentration will have an obvious influence on the water concentration in the membrane surface, and subsequently affect the diffusivity and flux.[53] Figure 7b reveals that the salt concentration increased from 3 wt.% (30 g/L) to 6wt.% (60 g/L), hence the water concentration decreased from 97 wt.% to 94 wt.%. The decreasing water concentration leads to a decrease in diffusivity in the membrane then water flux decreased. Table 2 summarizes several recent pervaporation membranes published in the literature.

Table 2. Comparison of pervaporation membranes in desalination of saline water

Membrane	Temperature in feed side (^{0}C)	NaCl conc. (g/L)	Flux (kg/m^2.h)	NaCl rejection (%)	Ref.
Cellulose triacetate	50	100	2.3	99	35
Cellulose triacetate /Al_2O_3	70	30 90	6.8 5	99.8	20
Cellulose triacetate /CNCs	70	30 90	11.67 7.6	99.7	42
Poly(vinyl alcohol)/maleic acid/TEOS	22	2	6.93	99.5	58
Poly(vinyl alcohol)/TEOS	Room temperature	2	96	99.9	59
Poly(vinyl alcohol)/TEOS/polysulfone	60	2 30	20.6 10.6	99.9	60
Cellulose triacetate/Ludox-SiO_2	70	30	6.1	99.8	This study

CONCLUSION

CTA/SiO_2 nanocomposie membranes were produced by solution casting for pervaporation desalination. The incorporation of SiO_2 in CTA membranes improved the mechanical strength of the membranes. The optimum SiO_2 added to CTA membrane was 4 wt.% and increased the water flux by a factor 2.5 compared to pristine CTA (from 2.2 kg m^{-2} h^{-1} to 6.1kg m^{-2} h^{-1}), while the salt rejection was 99.8% using a feed solution of 30 g/L aqueous NaCl at 70°C. The water flux decreased by 21% (6.1 kg m^{-2} h^{-1} to 4.8 kg m^{-2} h^{-1}) when the concentration of a feed solution rose from 30 g/L to 60 g/L. It can be concluded that the CTA/4wt.% SiO_2

nanocomposite membrane is a promising candidate for application in desalination by pervaporation.

ACKNOWLEDGEMENT

This work was supported by the Indonesia Endowment Fund for Education (LPDP). The authors would like to thank to Christine Wouters (KU Leuven) for measuring FTIR.

REFERENCES

1. Liu, G.; Shen, J.; Liu, Q.; Liu, G.; Xiong, J.; Yang, J.; Jin, W. *J. Memb. Sci.* **2018**, *548*, 548.
2. Greenlee Lauren F. A4 - Lawler, Desmond F. A4 - Freeman, Benny D. A4 - Marrot, Benoit A4 - Moulin, Philippe, L. F. A.-G. *Water Res.* **2009**, *v. 43*, pp. 2317.
3. Mayor, B. *Desalination* **2019**, *457*, 75.
4. McCutcheon, J. R.; McGinnis, R. L.; Elimelech, M. *Desalination* **2005**, *174*, 1.
5. Politano, A.; Argurio, P.; Di Profio, G.; Sanna, V.; Cupolillo, A.; Chakraborty, S.; Arafat, H. A.; Curcio, E. *Adv. Mater.* **2017**, *29*, 1603504.
6. Hartanto, Y.; Zargar, M.; Cui, X.; Jin, B.; Dai, S. *J. Memb. Sci.* **2019**, *572*, 480.
7. Zou, S.; Qin, M.; He, Z. *Water Res.* **2019**, *149*, 362.
8. Wang, J.; Gao, S.; Tian, J.; Cui, F.; Shi, W. *Water* **2020**, *12*, 692.
9. Tijing, L. D.; Woo, Y. C.; Choi, J.-S.; Lee, S.; Kim, S.-H.; Shon, H. K. *J. Memb. Sci.* **2015**, *475*, 215.
10. Wang, Q.; Li, N.; Bolto, B.; Hoang, M.; Xie, Z. *Desalination* **2016**, *387*, 46.
11. Prihatiningtyas, I.; Li, Y.; Hartanto, Y.; Vananroye, A.; Coenen, N.; Van der Bruggen, B. *Chem. Eng. J.* **2020**, *388*.
12. Cai, B.; Zhou, Y.; Gao, C. *Desalination* **2002**, *146*, 331.
13. Khorshidi, B.; Biswas, I.; Ghosh, T.; Thundat, T.; Sadrzadeh, M. *Sci. Rep.* **2018**, *8*, 1.

14. Thuyavan, Y. L.; Anantharaman, N.; Arthanareeswaran, G.; Ismail, A. F.; Mangalaraja, R. V. *Desalination* **2015**, *365*, 355.
15. Li, Y.-X.; Cao, Y.; Wang, M.; Xu, Z.-L.; Zhang, H.-Z.; Liu, X.-W.; Li, Z. *J. Memb. Sci.* **2018**, *565*, 322.
16. Zhang, Q.; Fan, L.; Yang, Z.; Zhang, R.; Liu, Y.; He, M.; Su, Y.; Jiang, Z. *Appl. Surf. Sci.* **2017**, *410*, 494.
17. da Silva, D. A. R. O.; Zuge, L. C. B.; de Paula Scheer, A. *Sep. Purif. Technol.* **2020**, 116852.
18. Zargar, M.; Hartanto, Y.; Jin, B.; Dai, S. *J. Memb. Sci.* **2017**, *541*, 19.
19. Abdelsamad, A. M. A.; Matthias, M.; Khalil, A. S. G.; Ulbricht, M. *Sep. Purif. Technol.* **2019**, *228*, 115767.
20. Prihatiningtyas, I.; Gebreslase, G. A.; Van der Bruggen *Desalination* **2020**, *474*, 114198.
21. Lin, Y.; Loh, C. H.; Shi, L.; Fan, Y.; Wang, R. *J. Memb. Sci.* **2017**, *539*, 65.
22. Ugur Nigiz, F. *Desalination* **2020**, *485*, 114465.
23. Liang, B.; Zhan, W.; Qi, G.; Lin, S.; Nan, Q.; Liu, Y.; Cao, B.; Pan, K. *J. Mater. Chem. A* **2015**, *3*, 5140.
24. Ali, S.; Rehman, S. A. U.; Luan, H.-Y.; Farid, M. U.; Huang, H. *Sci. Total Environ.* **2019**, *646*, 1126.
25. Yang, G.; Xie, Z.; Cran, M.; Ng, D.; Gray, S. *J. Memb. Sci.* **2019**, *579*, 40.
26. Selim, A.; Toth, A. J.; Haaz, E.; Fozer, D.; Szanyi, A.; Hegyesi, N.; Mizsey, P. *Sep. Purif. Technol.* **2019**, *221*, 201.
27. Kadhom, M.; Albayati, N.; Salih, S.; Al-Furaiji, M.; Bayati, M.; Deng, B. *Membr.* **2019**, *9*.
28. Asempour, F.; Emadzadeh, D.; Matsuura, T.; Kruczek, B. *Desalination* **2018**, *439*, 179.

29. Niang, M.; Luo, G. *Sep. Purif. Technol.* **2001**, *24*, 427.
30. Ma, X.; Hu, C.; Guo, R.; Fang, X.; Wu, H.; Jiang, Z. *Sep. Purif. Technol.* **2008**, *59*, 34.
31. Zhou, K.; Zhang, Q. G.; Han, G. L.; Zhu, A. M.; Liu, Q. L. *J. Memb. Sci.* **2013**, *448*, 93.
32. Bhat, N. V; Wavhal, D. S. *J. Appl. Polym. Sci.* **2000**, *76*, 258.
33. Rynkowska, E.; Dzieszkowski, K.; Lancien, A.; Fatyeyeva, K.; Szymczyk, A.; Kujawa, J.; Koter, S.; Marais, S.; Wolan, A.; Kujawski, W. *J. Memb. Sci.* **2017**, *544*, 243.
34. Naim, M.; Elewa, M.; El-Shafei, A.; Moneer, A. *Water Sci. Technol.* **2015**, *72*, 785.
35. Huth, E.; Muthu, S.; Ruff, L.; Brant, J. A. *J. Water Reuse Desalin.* **2014**, *4*, 109.
36. Kertész, S.; Freitas, T. B. de; Hodúr, C. *Analecta Tech. Szeged.* **2014**, *8*.
37. Boruah, A.; Rasheed, A.; Mendhe, V. A.; Ganapathi, S. *J. Pet. Explor. Prod. Technol.* **2019**, *9*, 1041.
38. Wang, T.; Ni, M. J.; Luo, Z. Y.; Shou, C. H.; Cen, K. F. *Chinese Sci. Bull.* **2012**, *57*, 3644.
39. Yu, F.; Chen, Y.; Liang, X.; Xu, J.; Lee, C.; Liang, Q.; Tao, P.; Deng, T. *Prog. Nat. Sci. Mater. Int.* **2017**, *27*, 531.
40. Duan, F.; Kwek, D.; Crivoi, A. *Nanoscale Res. Lett.* **2011**, *6*, 248.
41. Ashraf, M. A.; Peng, W.; Zare, Y.; Rhee, K. Y. *Nanoscale Res. Lett.* **2018**, *13*.
42. Prihatiningtyas, I.; Volodin, A.; Van der Bruggen, B. *Ind. Eng. Chem. Res.* **2019**, *58*, 14340.
43. Alayo, M. I.; Pereyra, I.; Scopel, W. L.; Fantini, M. C. A. *Thin Solid Films* **2002**, *402*, 154.
44. Pai, P. G.; Chao, S. S.; Takagi, Y.; Lucovsky, G. *J. Vac. Sci. Technol. A Vacuum, Surfaces, Film.* **1986**, *4*, 689.
45. Wenzel, R. N. *J. Phys. Colloid Chem.* **1949**, *53*, 1466.
46. Cassie, A. B. D.; Baxter, S. *Trans. Faraday Soc.* **1944**, *40*, 546.

47. Salahshoori, I.; Nasirian, D.; Rashidi, N.; Hossain, M. K.; Hatami, A.; Hassanzadeganroudsari, M. Springer Berlin Heidelberg, **2020**.
48. Heidary, M.; Jafari, S. H.; Khonakdar, H. A.; Wagenknecht, U.; Heinrich, G.; Boldt, R. *J. Appl. Polym. Sci.* **2013**, *127*, 1172.
49. Khdary, N. H.; Abdelsalam, M. E. *Arab. J. Chem.* **2020**, *13*, 557.
50. Zuo, X.; Shi, W.; Yu, S.; He, J. *Water Sci. Technol.* **2012**, *66*, 2343.
51. Kim, E.-S.; Deng, B. *J. Memb. Sci.* **2011**, *375*, 46.
52. Kull, K. R.; Steen, M. L.; Fisher, E. R. *J. Memb. Sci.* **2005**, *246*, 203.
53. Xie, Z.; Ng, D.; Hoang, M.; Duong, T.; Gray, S. *Desalination* **2011**, *273*, 220.
54. Singha, N. R.; Karmakar, M.; Chattopadhyay, P. K.; Roy, S.; Deb, M.; Mondal, H.; Mahapatra, M.; Dutta, A.; Mitra, M.; Roy, J. S. D. *Membranes (Basel).* **2019**, *9*.
55. Azadikhah Marian, S.; Asghari, M.; Amini, Z. *J. Water Environ. Nanotechnol. J. Water Environ. Nanotechnol* **2017**, *2*, 96.
56. Jiraratananon, R.; Chanachai, A.; Huang, R. Y. M.; Uttapap, D. *J. Memb. Sci.* **2002**, *195*, 143.
57. Thomson, G. W. M. **1946**, 1.
58. Xie, Z.; Hoang, M.; Duong, T.; Ng, D.; Dao, B.; Gray, S. *J. Memb. Sci.* **2011**, *383*, 96.
59. Chaudhri, S. G.; Rajai, B. H.; Singh, P. S. *RSC Adv.* **2015**, *5*, 65862.
60. Chaudhri, S. G.; Chaudhari, J. C.; Singh, P. S. *J. Appl. Polym. Sci.* **2018**, *135*, 1.